# Evaluation of an Innovative Pediatric Isolation Bed Using Fluid Dynamics Simulation and Physical Pollutants

**Tiantian Liu**
Guangdong Pharmaceutical University
**yubing guo**
Guangzhou Medical University
**xiaotang hao**
Guangdong Pharmaceutical University
**mei wang**
Guangdong Pharmaceutical University
**sicong he**
Guangzhou Medical University
**zhengshi lin**
Guangzhou Medical University
**rong zhou** ( zhourong@gird.cn )
Guangzhou Medical University

**Research**

**Keywords:** Computational fluid dynamics simulation (CFD), isolation bed, particles, speed, nosocomial infections, pediatrics

**Posted Date:** December 18th, 2019

**DOI:** https://doi.org/10.21203/rs.2.19286/v1

# Abstract

Background: Airborne transmission is an important mechanism of spread for both viruses and bacteria in hospitals, with nosocomial infections putting a great burden on public health. Patients in intensive care units are highly susceptible and these units by necessity already have incur high operating costs. Therefore, there is an urgent need for an economical medical device to prevent nosocomial infections. In order to achieve this goal, an innovative pediatric isolation bed was developed. Methods: We investigated the position of the child and air intake wind speed to test the local isolation effect of the bed using computational fluid dynamics simulation technology. Following this, we conducted purification experiments using cigarette smoke, and sustained release Staphylococcus albus and human adenovirus type 5 to demonstrate the isolation efficacy.

Results: The results showed that the patient's head should be placed as close to the air inlet hood as possible, and the value of air intake wind speed of 0.86 m/s was effective. The isolation efficacy of this innovative pediatric isolation bed is demonstrated by CFD technology and experiments using cigarette smoke and different kinds of microorganisms.

Conclusions: The pediatric isolation bed is mobile and economic, particularly useful for where infectious isolation wards are unavailable, such as in intensive care units and primary clinical settings, to control hospital acquired infection. This study provides a new method for the prevention and control of nosocomial infections.


# 1. Background

Nosocomial infections, known as hospital-acquired infections, are mainly caused by airborne pathogens and interpersonal contact in hospitals. It has been reported that the air in hospitals and other health service buildings contains microbial aerosols, and thus controlling the level of pathogenic microbial infections ensures the safety of workers and patient groups[1, 2]. At present, there are frequent outbreaks of epidemics caused by respiratory viruses[3, 4]. For example, norovirus is found seasonally in aerosols, as are avian influenza viruses[5, 6], with airborne transmission representing an important route of dissemination of H9N2 subtype avian influenza virus[7]. Furthermore, epidemic respiratory diseases have emerged in recent years, such as the severe acute respiratory syndrome epidemic in 2003, the H1N1 flu epidemic in 2011 and the Middle East Respiratory Syndrome epidemic in 2015[8–13]. Thus, it is vital to develop cost-effective non-pharmaceutical interventions that can prevent rather than treat such infections, and play a key role in the prevention and control of nosocomial infections[14, 15].

Measures to prevent and control nosocomial infections include engineering control strategies to reduce the risk of airborne infections. Although indoor air can spread pathogens, studies have shown that filtering or disinfecting air can reduce the risk of viral infections that are transmitted through the air[16]. A previous study simulated air flow trajectories and virus concentrations to assess airborne probability or risk of highly pathogenic avian influenza cases[2]. A further study demonstrated the effects of different

airflow patterns on droplet removal, identifying droplet carryover of infectious diseases, short- and long-range aerial propagation characteristics, and found that increasing ventilation rates can effectively reduce the risk of long-range airborne transmission;spread may therefore be inefficient, indicating that an effective way to prevent cross-contamination is to isolate the airflow[8].

Computational fluid dynamics (CFD) modeling can be used to assess whether hospital ultraviolet germicidal irradiation devices and ventilation systems are effective for infection control[5]. In our study, we used CFD simulation technology to investigate the position of the child and the air supply speed of the purification equipment when testing the local isolation effect of the pediatric isolation bed. Under laboratory conditions, isolation experiments with cigarette particles, sustained release Staphylococcus albus (S. albus) and human adenovirus type 5 (HAdV-5) demonstrated the efficacy of the isolation bed. This study provides new methods for the prevention and control of nosocomial infections.

# 2. Methods

2.1 Pathogens, cells and equipment

*Staphylococcus albus* was purchased from the Microbiology Institute of Guangdong (Guangdong, China). HAdV-5 was provided by the State Key Laboratory of Guangzhou (Guangzhou, China). *Escherichia coli* BJ5183 and Top 10 cells were purchased from Takara (Dalian, China). Cigarettes (Hongtashan, Yunnan, China) were purchased from a local retailer. Ad293 cells were cultured in Dulbecco's Modified Eagle's Medium (DMEM) containing penicillin-G 100 U/ mL, streptomycin 100μg/mL and 10% fetal bovine serum (Invitrogen, Carlsbad, CA, USA) and frozen using a BioFlash commercial freezing kit (Fibulas, New York, NY, USA). A Y09-301 laser dust particle counter and an Anderson six-level sampler were both purchased from Sujin (Jiangsu, China). Virus collection which specially collection the virus was purchased from Millipore (Millipore,MMAS,USA). Viruses were purified using standard CsCl isopycnic centrifugation.

2.2 Pediatric isolation bed

This new pediatric isolation bed was innervated by Guangzhou Angel biosafety Co.,Ltd. The bed is connected to a purification device that surrounds thechild's head, exhaled vapors from the child are directly drawn into the purification device that captures the harmful microorganisms by a sterilization filtering apparatus. The purified air is then blown back into the ward, providing patients with clean air, as well as reducing cross infections by air transmission among patients in the same ward. The purification device of the bed can be operated under three different wind speeds to create a negative pressure at the air inlet port, with high speed 0.86/ms, medium speed (0.55 m/s), and low speed (0.35 m/s), and can also be shut off (0 m/s) as a control. Compared with air quality controlled at the whole room level, the isolation bed reduces energy consumption and has enormous potential for application.

2.3 Geometry model establishment

The relevant parameters in the geometric model, including the size of the bed, the size of the purification equipment, and the size and position of the air inlet hood , were established according to the known parameters of the actual product, and were reasonably simplified. The specific parameters are shown in Table 1.

The air supply position had little effect on the simulation results, and different air supply positions are not discussed in this simulation.

To study the influence of the geometric relationship between the child and the air inlet hood on the effect of the intaking airflow,the angle θ was set at the child's mouth between the longitudinal axis of the body and the highest point of the air inlet hood, according to the equipment and children's geometrical shape in this case.

Actually the range of θ can be found to be approximately 44.8°–73.0°. Therefore, simulations and comparisons were performed by taking θ=50°, 60°, and 70°. The closer the child is to the air inlet hood, the larger θ is when the shape of the device is unchanged. The schematic θ and the meshing results of the model are shown in Figure 1 (taking θ=70° as an example). When θ was 50°, 60°, and 70°, the total number of body meshes was 3472824, 3341411, and 3487467, respectively. The mesh surrounding the human body was the densest, followed by the mesh around the bed, and the other mesh scatteringin the room were the most sparse.

2.4 Simulation condition settings

The effects of different relative positions and different purifying wind speeds on indoor wind speed, pressure and pollutant distribution were investigated in the simulation. The simulation conditions are shown in Table 2. Among them, according to the actual usage situation, the purifying air volume of the child's bed was 280 $m^3$/h, that is, the windspeed of the purifying equipment was 0.86 m/s, as represented in Case 6.

This simulation simplifies the patient's breathing state, considering only the patient's exhalation. The exogenous pathogenic microorganisms are represented by the tracer gas, $N_2O$.

2.5 calculation equations

The governing equations are given in a vector form as follows:

**See Formula 1 in the Supplemental Files**

Where ϕ is a general scalar quantity, which can represent u,v,w,k,e,T and tracer gas concentration. The diffusion coefficients Γ_ϕ and the source term S_ϕ for each scalar are summarized in Table 3-1. The tracer gas with a 4% volume fraction was added in the exhaled air of the source manikin. The properties of the tracer gas in the simulation were set the same as N2O which was used in the experiment. Only

steady state simulation was considered and the exhaled air was set at an average velocity of 0.86 m/s and a temperature of 25 ºC.

2.6 Validation experiment

A 30 $m^3$ test chamber was selected to simulate the size of a general ward room, and the isolation effect of the device in actual usage by means of exposure to artificial pollutants. The airflow wind speed using the results of the previous simulations was set at 0.86 m/s and θ=70°. The isolation bed was placed into the test chamber with a cigarette smoke generator release port or a microbial aerosol generator (bacterial and viral pathogens) placed 20 cm above the middle of the isolation bed. The horizontal distances from the wall were greater than 1 m, and the vertical distance from the ground was about 140 cm. The test was repeated three times and the average value of the pass efficiency was calculated. All tests were performed at 25°C–26°C, and the doors, windows, and air conditioners were all closed/off during the test.

2.6.1 Cigarette smoke

Using the smoke of a Hongtashan cigarette as a source of pollution, the cigarette was ignited and the cigarette-smoke generating device was activated. The release port was placed in position A (Figure 2), 20 cm above the bed, at a similar height to the face of the patient. Simultaneously, the purification device of the isolation bed was switched on. After 1 hour, the air was sampled at points A, B, C, D, E, F, G and H (Figure 2.), using a dust particle counter with a flow rate of 2.83 L/min and a sampling time of 20s.

2.6.2 Bacteria

Bacteria were cultured for between four and seven generations at 37°C for 24 h as indicator bacteria. A bacterial suspension with concertration 1.0 *$10^7$ cfu/ml was prepared and added to the microbial aerosol generator, which was activated and positioned with the release port at position A (Figure 2). Simultaneously, the purification device of the isolation bed was switched on. After 1 hour, the sampling port was positioned at points A, B, C, D, E, F, G and H (Figure 2). An Anderson six-stage sampler was used to collect and determine the concentration of microorganisms in the room at a flow rate of 28.3 L/min for 3 min. The sample plates were placed in an incubator at 37°C for 24 h to count the colonies and calculate the concentration of microorganisms in the air.

2.6.3 Viruses

HAdV-5 was cultured in AD293 cells, purified and stored at −80°C. The 50% tissue culture infective dose of the virus was determined following the routine procedure, as previously described [17]. Purified HAdV-5 was dilution with PBS to prepare a mixed-pathogen suspension, which was placed in the activated microbial aerosol generator with the release port at position A (Figure 2). Simultaneously, the isolation bed was switched on. After 1 hour, air samples were taken with the sampling port positioned at A, B, C, D, E, F, G and H (Figure 2).A virus collection was used to collect virus. and determine the concentration of virus in the room at a flow rate of 100 L/min for 10 min. The number of viral genome copies at each time

point was determined by real-time quantitative PCR (Q-PCR) using a universal adenovirus Q-PCR kit (Hexin Corporation, Guangzhou, China) on an Applied Biosystems 7500 real-time PCR system (Foster City, CA). Each assay was performed three times in duplicate. The quantification of the genome copy numbers of HAdV-5 was performed with HAdV type specific primers and purified HAdV genomic DNA as the standard curve.We obtain the template genomic DNA from Pubmed.

2.7 Statistical analysis

Statistical analysis was performed by t-test, using Prism 7 software (GraphPad, San Diego, CA, USA). P values (P) less than 0.05 were considered statistically significant.

# 3. Results

3.1 Influence of the relative position of the child and intake airflow (θ) on the isolation effect.

The angle θ, as defined above,was set at 50°, 60° and 70° respectively for simulation and comparison in Cases 1, 2, and 3, respectively, and the intake airflow speed of the purification equipment was maintained at 1 m/s. The pressure distribution is shown in Figure 3, velocity distribution is shown in Figure 4, and the tracer gas mass fraction distribution is shown in Figure 5.

It can be seen from Figure 3 that a slight negative pressure was formed around the air intake vent; the negative pressure on the surface of the air intake vent was about -0.8 Pa, and a slight negative pressure was present in the range of about 30 cm around the air intake vent. Figure 4 shows that the indoor airflow velocity fields of the three scenarios were similar because the air intake wind speed of the purification device was kept the same. It can be seen from Figure 5 that the tracer gas concentration in the room was maintained at a low level in all three cases, and the air inlet hood effectively controlled the discharged pollutants ($N_2O$), indicating that the isolation effect was good. In addtion, as the distance between the child's headand the hood decreased, the concentration of tracer gas in the indoor air was further reduced. Therefore, the shorter the distance between the child's head and the return hood, the more efficient the isolation effect.

3.2 Influence of airintaking wind speed on the isolation effect of the purification equipment.

The effect of air intaking wind speeds of 1 m/s, 2 m/s, 3 m/s, 0.86 m/s on isolation effect was investigated in Cases 3, 4, 5, and 6, respectively, with θ remaining at 70°. The pressure distribution is shown in Figure 6, velocity distribution is shown in Figure 7 and distribution of the mass fraction of the tracer gas is shown in Figure 8.

The simulation results show that the air intaking wind speed of the purification equipment was 0.86 m/s, which is close to the case of 1 m/s. Figure 6 shows that as the air supply volume increased, the corresponding return air volume also increased, so the negative pressure formed locally near the return air vent gradually increased. The negative pressures on the surface of the return air inlets of Case 3 and

Case 6 were approximately -0.8 Pa, while the negative pressures on the surface of the return port in Cases 4 and 5 were about -3.4 Pa and -7.6 Pa, respectively, indicating that the area of negative pressure around the air return port was gradually enlarged. Figure 7 shows that as the wind speed of the air supply increased, the degree of turbulence of the indoor air increased. It can be seen from Figure 8 that because the distance between the head of the child and the returning hood was very short, even if the wind speed of the air supply was great, the vigorous movement of the indoor air did not impede the trajectory of the pollutants, and the pollutants were always removed timeously. Thus the intended isolation effect was obtained and the rationale of the return hood design was justified. The greater the wind speed, the smaller the area of local infection risk, but the energy consumption must increase accordingly, as will the likelihood of patient discomfort caused by hair movement. Therefore, to meet the purification requirements, a larger supply/return wind speed should be used whenever possible, but energy consumption and comfort must also be considered. At the current supply wind speed of 0.86 m/s, the concentration of pollutants in the region surrounding the patient's head is higher, which conveys a certain risk of infection.

### 3.3. Experimental validation

To validate the results of the CFD, we used cigarette smoke (Figure 9A), *Staphylococcus albus* (Figure 9B) and HAdV-5 (Figure 9C) to test the isolation efficiency of the isolation bed at an air intake wind speed of 0.86 m/s. As shown in Figure 9A, position A is the point of origin of the pollutant. Therefore, numerical values of point A was the highest in terms of the number of cigarette particles, bacteria and genome copies of viruses. As shown in Figure 9A, the numbers of particles detected in the rest of the room (including both sides of the bed and the foot of the bed) were significantly lower than those found at position A（$P<0.01$）, and actually below the levels found in a normal room (data not shown). Consistent with this, Figure 9B and C show that the numbers of bacteria and viruses, respectively, in the rest of the room (including both sides and the foot of the bed) were significantly lower than those detected at point A（$P<0.01$） being lower than the minimum detectable bacterial content required by hospital wards, or undetectable, in the case of viral genomes.

## 4. Discussion

Effective isolation equipment is vital for protection of both patients and staff, particularly in intensive care settings. We used a CFD model and physical validation methods to investigate the efficacy of a new design of pediatric isolation bed. At the recommended air intake wind speed of 0.86 m/s, we found that pollutants were satisfactorily removed from the area surrounding the child's head, and that the return air circulated back into the room was free of pollutants. We also found that increasing the air intake wind speed and increasing the angle between the height of the child's face and the air return port (angle θ) resulted in improved isolation effect. We also found that a local negative pressure was formed around the return air hood. The specific values and presentation range of the negative pressure were related to the air supply volume/return air volume.

The influence of the relative position of the child and the return air on the isolation effect was investigated by varying the values of θ. The simulation results showed that the larger θ, that is, the shorter the distance between the child and the return hood, the lower the tracer gas concentration in the indoor space, the smaller the influence range, and the better the isolation effect. The larger the air supply volume/return air volume, the better the control effect of exhaled pollutants. Because the patient's head was positioned close to the return air outlet, severe turbulence did not impede the elimination of pollutants. However, the greater the wind speed, the greater the energy consumption and the stronger the blowing sensation felt by the patient. Therefore, a suitable wind speed should be chosen to meet purification, energy and comfort requirements. At the manufacturer-recommended air supply speed of the purification equipment (0.86 m/s), the concentration of pollutants in the area surrounding the patient's head was higher, and the concentration of pollutants in most areas of the room was lower than the levels detected at other air supply speeds.

We also validated the CFD results by sampling pollutant levels in and around the isolation bed using cigarette smoke, S. albus and HAdV-5 as pollutants. Regarding particle size, droplets have traditionally been defined as being > 5 μm in size [18, 19]. We tested the isolation efficiency against particles of 0.5–10.0 μm in size. It was found that the measured results were consistent with the CFD simulation values at this particle size. We also investigated the efficacy against 0.7 μm diameter S. albus and HAdV5, with a diameter of 0.1 μm. We found that the detected levels of S. albus were lower than the minimum required by hospital wards around the bed and throughout the room. Furthermore, we could not detect any virus in the room or around the bed. The above experimental results confirm the findings of our CFD model and demonstrate the isolation efficacy of this pediatric isolation bed for protection against particulate and pathogenic pollutants.

# 5. Conclusion

In summary, it can be seen from the simulation results that the design of the return hood is suitable, and the pollutants exhaled by the patient are sufficiently removed before air recirculation. It should be noted that the patient's head should be placed as close to the return air hood as possible, and a suitable and comfortable wind speed value should be determined. We also validated the isolation efficacy by sampling pollutant levels in and around the isolation bed using cigarette smoke, S. albus and HAdV-5 as pollutants. Our results are of great significance for treatment of patients in infectious disease and pediatric wards, among others. Next, the clinical impact of this device on reduction of nosocomial and cross infections between patients, medical staff and their families should be investigated, thus establishing its capacity to make a major contribution to public health.

# Declarations

### Ethics approval and consent to participate

Not applicable.

### Consent for publication

Not applicable.

### Availability of data and materials

The datasets used in the current study are available from the corresponding author on request.

### Competing interests

The authors declare that they have no competing interests.


### Funding

This study was supported by grants from National Key Research and Development Program of China (2018YFC1200100), Guangdong Medical Science and Technology Research Center Projec (A2019460), Entrepreneurship Leadership Project in Guangzhou Development Zone of China (CY2018-003), Guangzhou science and technology project (201704020225).


### Authors' contributions

RZ ,TL and SL were involved in the cinception and design of the study. TL YG, XH, MW and SH were involved in the acquisition of data. TL and SL analyzed the date. TL wrote the manuscript.


### Acknowledgements

Thanks for Prof. Qian Hua(School of Energy and Environment Southeast University, Nanjing, China) help us to do the CFD models.



### Authors' information (optional)

[1]School of Public Health, Guangdong Pharmaceutical University, Guangzhou, Guangdong 510310, China.

[2] State Key Laboratory of Respiratory Disease, National Clinical Research Center for Respiratory Disease, Guangzhou Institute of Respiratory Health, First Affiliated Hospital of Guangzhou Medical University, Guangzhou Medical University, Guangzhou, China.


### Declaration of Competing Interest

No.

## Abbreviations

CFD :Computational fluid dynamics; S. albus :Staphylococcus albus; HAdV-5: human adenovirus type 5

# References


1. Lanzerstorfer A, Hackl M, Schlomer M, Rest B, Deutsch-Grasl E, Lanzerstorfer C: **The influence of air-dispersed essential oils from lemon (Citrus limon) and silver fir (Abies alba) on airborne bacteria and fungi in hospital rooms**. *Journal of environmental science and health Part A, Toxic/hazardous substances & environmental engineering* 2019, 54(3):256-260.
2. Ai Z, Hashimoto K, Melikov AK: **Airborne transmission between room occupants during short-term events: Measurement and evaluation**. *Indoor air* 2019, 29(4):563-576.
3. Sivagnanasundaram P, Amarasekara RWK, Madegedara RMD, Ekanayake A, Magana-Arachchi DN: **Assessment of Airborne Bacterial and Fungal Communities in Selected Areas of Teaching Hospital, Kandy, Sri Lanka**. *BioMed research international* 2019, 2019:7393926.
4. Xiao S, Tang JW, Li Y: **Airborne or Fomite Transmission for Norovirus? A Case Study Revisited**. *International journal of environmental research and public health* 2017, 14(12).
5. Shiu EYC, Leung NHL, Cowling BJ: **Controversy around airborne versus droplet transmission of respiratory viruses: implication for infection prevention**. *Current opinion in infectious diseases* 2019, 32(4):372-379.
6. Alsved M, Fraenkel CJ, Bohgard M, Widell A, Soderlund-Strand A, Lanbeck P, Holmdahl T, Isaxon C, Gudmundsson A, Medstrand P *et al*: **Sources of Airborne Norovirus in Hospital Outbreaks**. *Clinical infectious diseases : an official publication of the Infectious Diseases Society of America* 2019.
7. Su H, Yang X, Wang S, Shi H, Liu X: **Effect of annexin II-mediated conversion of plasmin from plasminogen on airborne transmission of H9N2 avian influenza virus**. *Veterinary microbiology* 2018, 223:100-106.
8. Qian H, Zheng X: **Ventilation control for airborne transmission of human exhaled bio-aerosols in buildings**. *Journal of thoracic disease* 2018, 10(Suppl 19):S2295-S2304.
9. Bertran K, Balzli C, Kwon YK, Tumpey TM, Clark A, Swayne DE: **Airborne Transmission of Highly Pathogenic Influenza Virus during Processing of Infected Poultry**. *Emerging infectious diseases* 2017, 23(11):1806-1814.
10. Fujiyoshi S, Tanaka D, Maruyama F: **Transmission of Airborne Bacteria across Built Environments and Its Measurement Standards: A Review**. *Frontiers in microbiology* 2017, 8:2336.
11. Hella J, Morrow C, Mhimbira F, Ginsberg S, Chitnis N, Gagneux S, Mutayoba B, Wood R, Fenner L: **Tuberculosis transmission in public locations in Tanzania: A novel approach to studying airborne disease transmission**. *The Journal of infection* 2017, 75(3):191-197.
12. Richard M, Herfst S, van den Brand JMA, de Meulder D, Lexmond P, Bestebroer TM, Fouchier RAM: **Mutations Driving Airborne Transmission of A/H5N1 Virus in Mammals Cause Substantial Attenuation in Chickens only when combined**. *Scientific reports* 2017, 7(1):7187.
13. Tong X, Xu H, Zou L, Cai M, Xu X, Zhao Z, Xiao F, Li Y: **High diversity of airborne fungi in the hospital environment as revealed by meta-sequencing-based microbiome analysis**. *Scientific reports* 2017, 7:39606.

14. Gosce L, Johansson A: **Analysing the link between public transport use and airborne transmission: mobility and contagion in the London underground**. *Environmental health : a global access science source* 2018, 17(1):84.
15. Xu P, Fisher N, Miller SL: **Using computational fluid dynamics modeling to evaluate the design of hospital ultraviolet germicidal irradiation systems for inactivating airborne mycobacteria**. *Photochemistry and photobiology* 2013, 89(4):792-798.
16. Tang JW, Li Y: **Editorial: the airborne microbiome - implications for aerosol transmission and infection control - special issue**. *BMC infectious diseases* 2019, 19(1):755.
17. Liu T, Zhou Z, Tian X, Liu W, Xu D, Fan Y, Liao J, Gu S, Li X, Zhou R: **A recombinant trivalent vaccine candidate against human adenovirus types 3, 7, and 55**. *Vaccine* 2018, 36(16):2199-2206.
18. Siegel JD, Rhinehart E, Jackson M, Chiarello L, Health Care Infection Control Practices Advisory C: **2007 Guideline for Isolation Precautions: Preventing Transmission of Infectious Agents in Health Care Settings**. *American journal of infection control* 2007, 35(10 Suppl 2):S65-164.
19. La Rosa G, Fratini M, Della Libera S, Iaconelli M, Muscillo M: **Viral infections acquired indoors through airborne, droplet or contact transmission**. *Annali dell'Istituto superiore di sanita* 2013, 49(2):124-132.

# Tables

Table 1. Parameters of the geometric model

| Term | Size | Hydraulic diameter (m) | Temperature | Iteam |
|---|---|---|---|---|
| Testing room | 5.0 m(x)×4.0 m(z)×3.0 m(y) | — | — | — |
| patient's mouth[a] | | 0.012 m | — | |
| Air intake ports[b] | total 0.0593 $m^2$ | — | | 126 |
| Air supply port[c] | 0.0903 $m^2$ | 0.288 m | 25°C | — |
| Exhalation | — | — | 33°C | — |
| Patient's skin | — | — | 40 $W/m^2$ （fever） | — |

Note：

a: The child’s head was set at the horizontal center of the room;

b: The number and size of the air intake ports were determined from the stp file;

c: To facilitate the mesh division and ensure the quality of the mesh, the small air outlets of the air supply port were merged into one large air outlet, so the air supply area was simulated. It was larger than the data on the computer-aided design drawings, but had little effect on the simulation results.

Table 2. Simulation condition settings

| Case | Patient exhalation situation | θ | Wind current speed of the purification equipment (m/s) |
|---|---|---|---|
| 1 | Exhalation speed 1 m / s, tracer gas mole fraction 0.04 (mole fraction is about 0.06) | 50° | 1 |
| 2 | | 60° | 1 |
| 3 | | 70° | 1 |
| 4 | | 70° | 2 |
| 5 | | 70° | 3 |
| 6 | | 70° | 0.86 |

## Figures

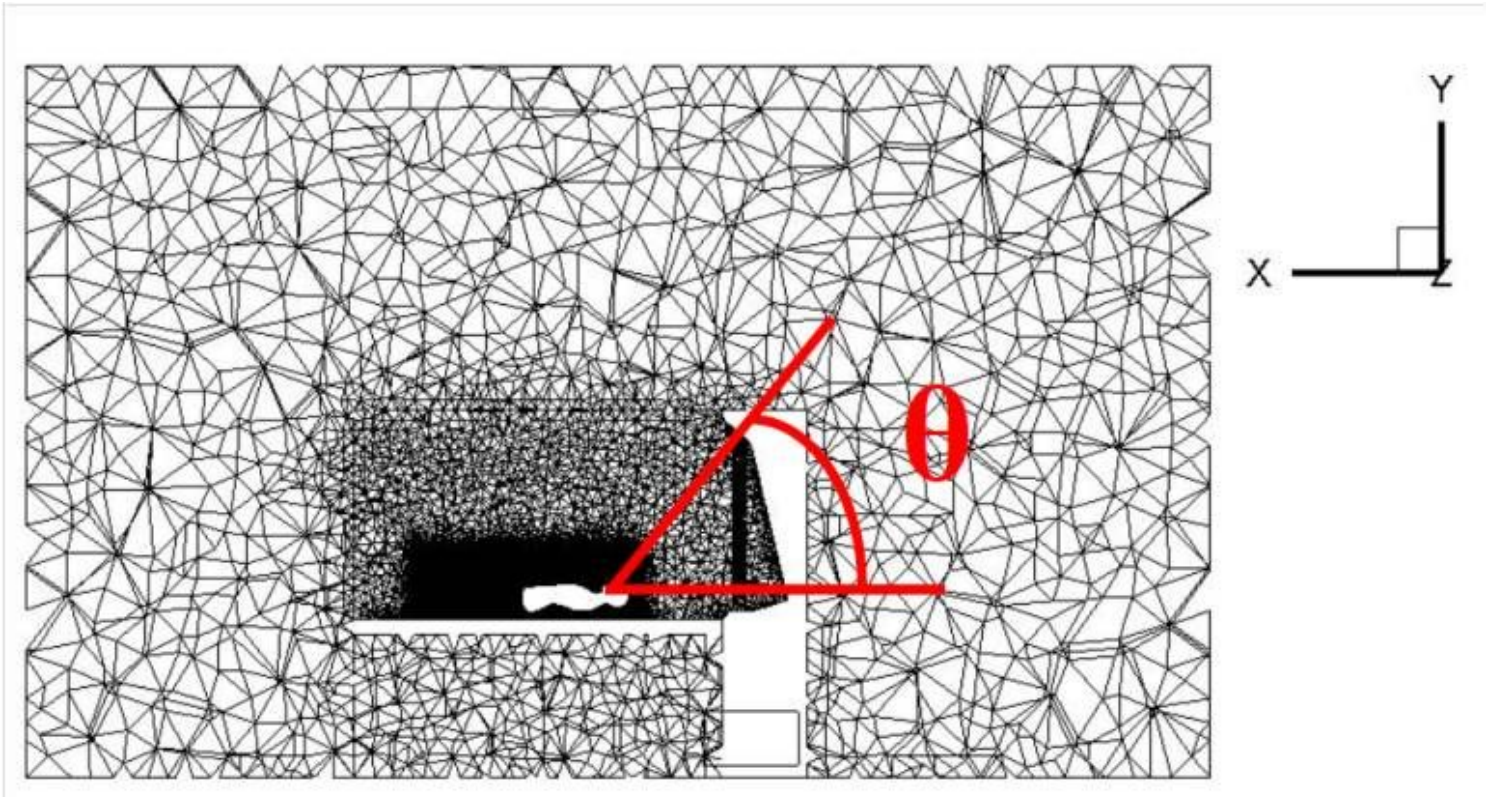


**Figure 1**

Schematic diagram of mesh generation. θ=70° in the diagram.

**Figure 2**

Sampling sites within the room during isolation bed testing.

**Figure 3**

Pressure distribution. A. Case 1, θ=50°; B. Case 2, θ=60°; C. Case 3, θ=70°.

**Figure 4**

Speed distribution. A. Case 1, θ=50°; B. Case 2, θ=60°; C. Case 3; θ=70°. A1, B1, C1: longitudinal view; A2, B2, C2: transverse view.

**Figure 5**

Tracer gas mass fraction distribution. A. Case 1, θ=50°; B. Case 2, θ=60°; C. Case 3, θ=70°.

**Figure 6**

Pressure distribution. A. Case 3, 1 m/s; B. Case 4, 2 m/s; C. Case 5, 3 m/s; D. Case 6, 0.86 m/s.

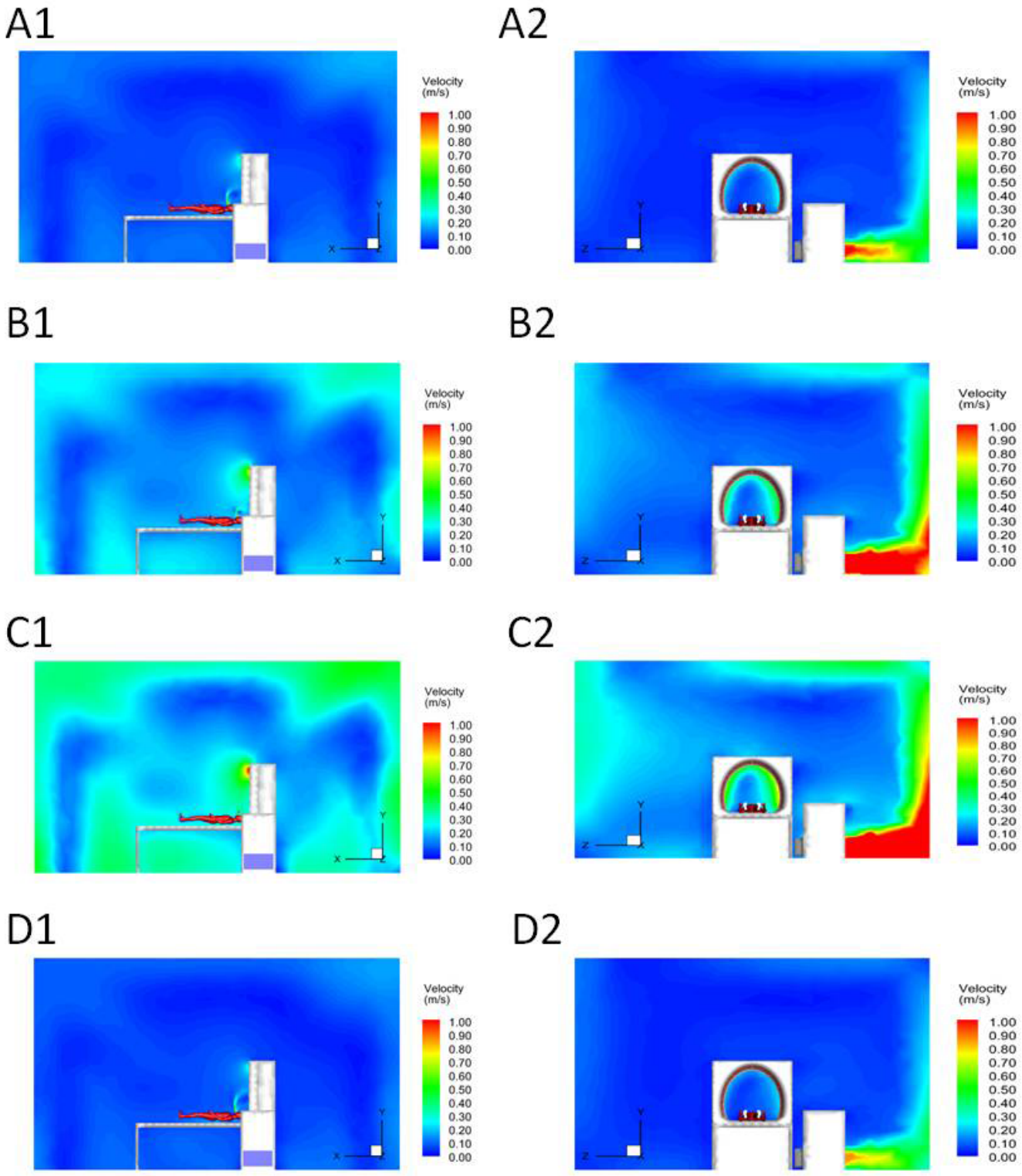


**Figure 7**

Speed distribution. A. Case 3, 1 m/s; B. Case 4, 2 m/s; C. Case 5, 3 m/s; D. Case 6, 0.86 m/s. A1, B1, C1 D1: longitudinal view; A2, B2, C2, D2: transverse view.

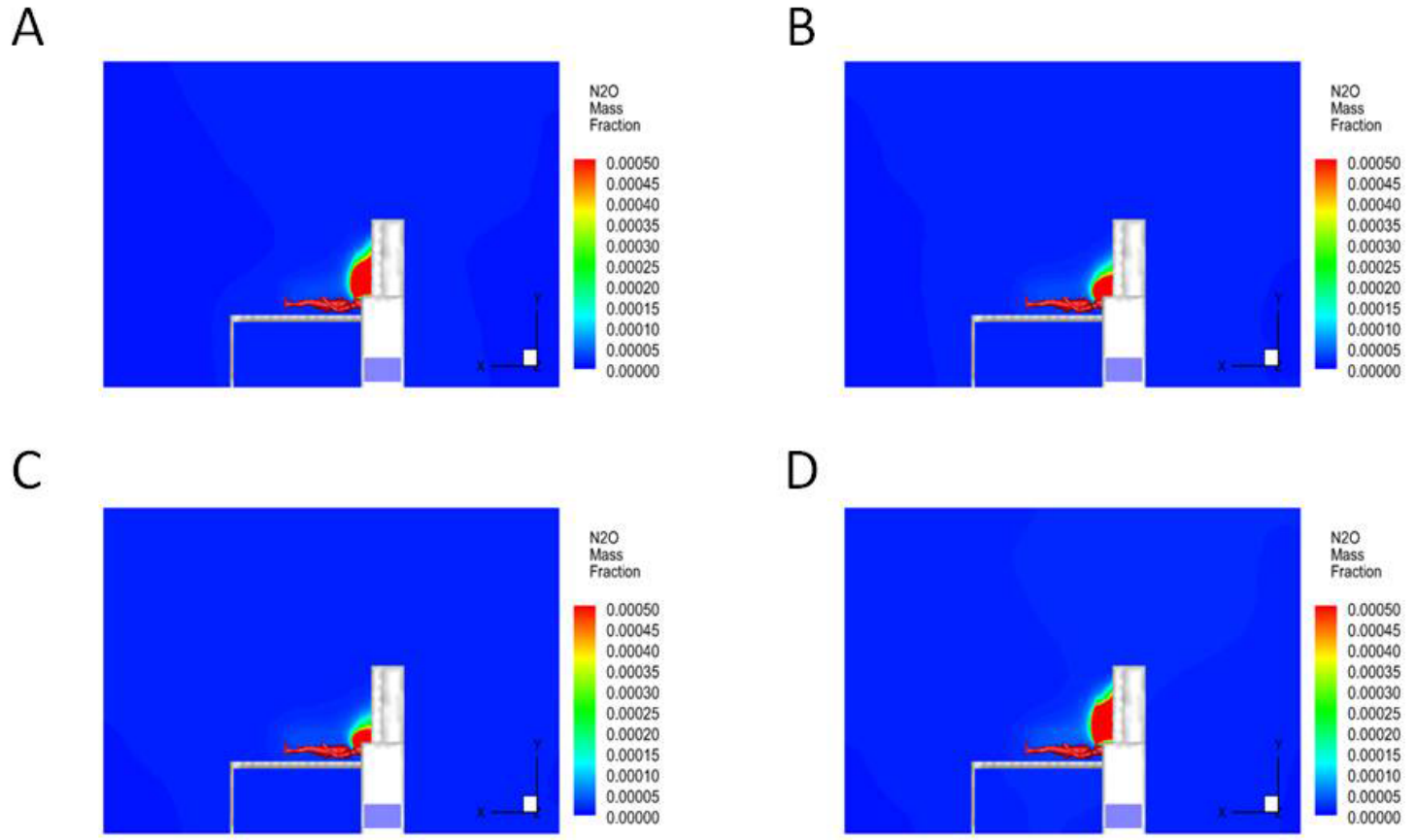


## Figure 8

Tracer gas mass fraction distribution. A. Case 3, 1 m/s; B. Case 4, 2 m/s; C. Case 5, 3 m/s; D. Case 6, 0.86 m/s.

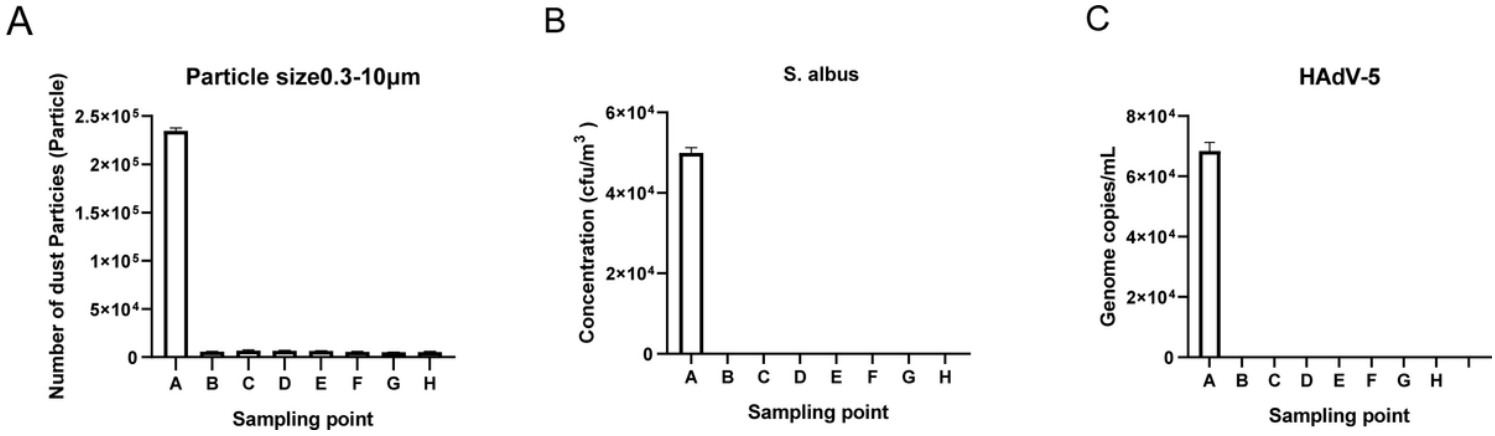


## Figure 9

Efficacy of the isolation bed. A. Cigarette smoke; B. Staphylococcus albus ; C. HAdV-5.